applied sciences

MDPI

*Article*

# Spinning of Endless Bioactive Silicate Glass Fibres for Fibre Reinforcement Applications

**Julia Eichhorn [1], Cindy Elschner [2], Martin Groß [1], Rudi Reichenbächer [2], Aarón X. Herrera Martín [3], Ana Prates Soares [3,4], Heilwig Fischer [3,4], Julia Kulkova [5], Niko Moritz [5], Leena Hupa [6], Markus Stommel [2,7], Christina Scheffler [2,*] and Martin Kilo [1]**

[1] Institute of Glass and Glass Technology, TU Bergakademie Freiberg, Akademiestraße 6, D-09599 Freiberg, Germany; julia.eichhorn@igt.tu-freiberg.de (J.E.); martin.gross@igt.tu-freiberg.de (M.G.); martin.kilo@igt.tu-freiberg.de (M.K.)
[2] Leibniz-Institut fuer Polymerforschung e. V., Hohe Straße 6, D-01069 Dresden, Germany; elschner@ipfdd.de (C.E.); reichenbaecher@ipfdd.de (R.R.); stommel@ipfdd.de (M.S.)
[3] Julius Wolff Institut, Berlin Institute of Health, Charité-Universitätsmedizin Berlin, Augustenburger Platz 1, D-13353 Berlin, Germany; aaron.herrera@bih-charite.de (A.X.H.M.); ana.prates-soares@charite.de (A.P.S.); heilwig.fischer@charite.de (H.F.)
[4] Department of Oral and Maxillofacial Surgery, Charité-Universitätsmedizin Berlin, Corporate Member of Freie Universität Berlin, Humboldt-Universität zu Berlin and Berlin Institute of Health, Augustenburger Platz 1, D-13353 Berlin, Germany
[5] Institute of Dentistry, University of Turku, Itäinen Pitkäkatu 4B (PharmaCity), FI-20520 Turku, Finland; julia.kulkova@utu.fi (J.K.); niko.moritz@utu.fi (N.M.)
[6] Laboratory of Molecular Science and Engineering, Faculty of Science and Engineering, Åbo Akademi University, Tuomiokirkontori 3, FI-20500 Turku, Finland; leena.hupa@abo.fi
[7] Institute of Material Science, Faculty Mechanical Engineering, Technical University Dresden, D-01062 Dresden, Germany
* Correspondence: scheffler@ipfdd.de

**Abstract:** Bioactive glasses have been used for many years in the human body as bone substitute. Since bioactive glasses are not readily available in the form of endless thin fibres with diameters below 20 µm, their use is limited to mainly non-load-bearing applications in the form of particles or granules. In this study, the spinnability of four bioactive silicate glasses was evaluated in terms of crystallisation behaviour, characteristic processing temperatures and viscosity determined by thermal analysis. The glass melts were drawn into fibres and their mechanical strength was measured by single fibre tensile tests before and after the surface treatment with different silanes. The degradation of the bioactive glasses was observed in simulated body fluid and pure water by recording the changes of the pH value and the ion concentration by inductively coupled plasma optical emission spectrometry; further, the glass degradation process was monitored by scanning electron microscopy. Additionally, first in vitro experiments using murine pre-osteoblast cell line MC3T3E1 were carried out in order to evaluate the interaction with the glass fibre surface. The results achieved in this work show up the potential of the manufacturing of endless bioactive glass fibres with appropriate mechanical strength to be applied as reinforcing fibres in new innovative medical implants.

**Keywords:** glass fibre spinning; bioactive glass fibres; surface modification; silanes



**Citation:** Eichhorn, J.; Elschner, C.; Groß, M.; Reichenbächer, R.; Herrera Martín, A.X.; Soares, A.P.; Fischer, H.; Kulkova, J.; Moritz, N.; Hupa, L.; et al. Spinning of Endless Bioactive Silicate Glass Fibres for Fibre Reinforcement Applications. *Appl. Sci.* **2021**, *11*, 7927. https://doi.org/10.3390/app11177927

Academic Editor: Chiara Soffritti

Received: 30 July 2021
Accepted: 23 August 2021
Published: 27 August 2021



## 1. Introduction

Glass as a transparent, smooth and chemically stable material has become an indispensable part of everyday life. By definition, glasses are solidified melts without crystallisation. When such a supercooled liquid is cooled to lower temperatures, its viscosity increases and the molecules move slower and slower until the structure is "frozen". This means that the time scales for molecular rearrangements are extremely long compared to the time period of experimental observation, but they can still take place. Glass is characterized by being a hard solid, but lacking an internal structure. When a substance lacks a crystal structure it

is referred to as amorphous. In contrast to the regular three-dimensional arrangement of the building blocks in crystals (long-range order), in glasses there are only orders in small domains (short-range order). When heated, they therefore do not melt above a certain temperature, but soften gradually [1].

In general, glasses consist of network formers, such as silica ($SiO_2$), boron trioxide ($B_2O_3$) or phosphorous pentoxide ($P_2O_5$), and network modifiers, which are one or several alkali and alkaline earth oxides. In addition, intermediate oxides, e.g., zirconium oxide ($ZrO_2$), aluminum oxide ($Al_2O_3$) can be present as a third class of constituents, which then act either as network modifiers or as network formers [2]. Therefore, glass properties are determined by the composition of the glass and the manufacturing (especially the cooling rate) and are also closely associated with its surface characteristics.

Typical applications, where corrosion of glass surfaces is particularly relevant, were identified by Hench & Clark [3] as follows: stability of glass containers and windows, leaching of nuclear waste encapsulants, preservation of glass antiquities, reliability of fibre optic interfaces, bonding of bioglasses to living tissues and environment sensitivity in fracture mechanics. As glass corrosion occurs, hydration, hydrolysis of the ionic covalent network, and exchange between ions, especially from the network modifiers and intermediate oxides and protons in solution, are closely related. Depending on the glass composition and on the surrounding conditions, various secondary phases may precipitate from dissolved elements. In most cases, an amorphous, hydrated layer, commonly referred to as a "gel", forms on the surface, with thickness ranging from nanometer range up to the macroscopic scale [4]. According to Hench and Clark, silicate glasses can be assigned into five categories. Class I to III glasses are considered stable systems. Class I provides the best water resistance. These glasses are almost inert and form a hydrated layer less than 5 nm thick. On class II glasses a silica-rich protective film is deposited due to selective alkali ion removal. The formation of to passivating layers is characteristic of class III glass surfaces. Glasses with additional $Al_2O_3$ or $P_2O_5$ are able to precipitate either alumina-silicate or calcium-phosphate species on top of a silica-rich layer which can be very durable. Compositions of class IV and V are designated as hydrolytically active glasses. Surfaces of class IV glasses do not show any passivating effect. These glasses have a comparatively low silica content. In contrast, the glass systems that are most unstable to aqueous solutions dissolve faster than a gel layer can form and represent class V. Such glasses are undergoing congruent dissolution with nearly equal loss of ions [3].

Hydrolytically active glasses have been in technical use for a long time. The group of water glasses are well-known representatives. These are alkaline sodium silicate solutions that react with soluble salts and salt solutions forming solids. For example, water glasses are used as adhesives and bleaching agents in the paper industry, as binders for mineral paints or as particle-free grout for sealing masonry [5]. Moreover, borosilicate glasses with a high alkali content, as well as many other borate glasses, have very good solubility. This is applied for the production of so-called Vycor-brand glass, in which porous glass with a high $SiO_2$ content is produced by extracting a borate segregation phase [6].

An exceptional variety of applications is offered by bioactive glasses, which are also classified as hydrolytically active. Searching for a material that could form a direct contact with the bone without being encapsulated in fibrous tissue, the first bioactive glass was discovered by Larry Hench in 1969. The hypothesis underlying his work involved the fact that a material capable of forming a bone-like hydroxyapatite (HAp) layer on its surface should not be rejected by the body, as HAp is the main mineral phase of natural bone tissue. The glass composition $45SiO_2$-$24.5Na_2O$-$24.5CaO$-$6P_2O_5$ (wt%) is referred to as 45S5 and it was trademarked under the name Bioglass® by the University of Florida [7]. Since the discovery of 45S5 glass, many other bioactive glass (BG) compositions have been developed. These are not silicate glasses alone, but also borate glasses, which, as already mentioned, exhibit particularly high dissolution rates and, in addition, the ability to form apatite, as well as phosphate glasses, which exhibit less pronounced bioactivity but high solubility as soon as they come into contact with biological fluids. Alongside their ability

to form hydroxyapatite-like surface layers after being put in contact with biological fluids, BG are also osteoinductive, i.e., they are able to stimulate bone cells, thus significantly accelerating tissue healing for both, hard and soft tissue, stimulate angiogenesis and inhibit bacterial growth [7–10].

In the vast majority of applications, medical products made of and containing bioactive glass are offered as powders or granules. Products with short, randomly oriented fibres that can be loaded with antibacterial agents and growth factors are serving as wound dressings [10]. Despite the success of commercially available, granular bioactive glasses used as bone substitute, they suffer from a few drawbacks as a defined and enclosed cavity is always required for the application. Otherwise, migration of the material into the surrounding tissue will occur [11,12]. Easier to handle than particles are 3D porous scaffolds [13], composite materials in which the glass particles [14,15] or short fibres [16] are embedded in biocompatible polymers [17], scaffolds with disordered fibre orientation created by electrospinning [10] or melt-derived microfibres [18].

Continuous fibres made from bioactive glasses that can be processed into textiles would be very attractive for numerous medical applications. For example, they might serve as reinforcing fibres in resorbable polymers, which could offer exciting prospects for load-bearing implants, as studied by Plyusnin et al. [19]. Moreover, textiles made of BG would also be a promising option for wound closure and may additionally be loaded with ions to specifically promote tissue regeneration. Furthermore, flexible, porous and customised scaffolds for tissue engineering could be produced from fibres.

Textile glass fibres can be made from strong viscous melts with melt spinning by downdrawing from bushing tips (Figure 1). Glass fibre formation involves a combination of extrusion and attenuation. During extrusion, the molten glass exits through a bushing made of an erosion-resistant platinum/rhodium alloy with very fine orifices. The winders apply tension to the glass, drawing it out into thin filaments. These are cooled by water spray, coated with a sizing and gathered together to form a strand. The most important melt properties are: the fibre-forming viscosity ($\eta$) that is quoted between $10^{1.8}$ to $10^{2.5}$ Pa·s and its corresponding temperature, the liquidus temperature at which crystals can form within hours and remain in equilibrium in melt and the processing temperature range, that is the difference between fibre-forming and liquidus temperature. To ensure a stable fibre spinning process, the processing window ($\Delta$T) should be at least 70 K [20,21]. Finally, a chemical coating, or sizing, is applied. Sizings are indispensable for textile fibres, regardless of their nature. These aqueous dispersions of film formers, adhesion promoters and modifiers are applied to the surface during the spinning process, where they form a protective layer. They are important for the textile processability of the fibres since they establish contact between the individual filaments, reduce roughness and thus improve the sliding properties on thread-carrying machine parts, increase strength and also enable bonding between the glass fiber and the polymer matrix. On the other hand, the silane-containing sizings are known to increase the strength of the fibres by bridging defects in the glass network [22,23].

Obtaining fibres from bioactive silicate glasses is challenging because of the narrow processing range of many BGs. That means that these glasses tend to segregate and crystallise during preparation, making it difficult to maintain the glass in an amorphous state. The devitrification tendency can be explained by their highly disrupted silicate network with low network connectivity. Due to the high concentration of non-bridging oxygen atoms, the covalent cross-linking between the silicate chains is reduced resulting in an increased mobility of the structural units, which facilitates rearrangement to form nuclei of critical size. Overall, it can be concluded that an increasing ratio of alkali/alkaline earth metal cations increases the crystallisation tendency and, moreover, prevents a stable drawing process. Additionally, their bioactivity is lowered [2,24]. Arstila et al. [25] showed that BG can be split into two groups, those that crystallise to sodium-calcium silicates such as combeite, ($Na_2O$-2CaO-3$SiO_2$) and those that crystallise to wollastonite (CaO-$SiO_2$), with the latter having a significantly increased processing window of 300 K compared to the

previous mentioned value. This shows that BG with high contents of sodium, such as 45S5, are less favourable for processing, while glasses with low contents, such as 13-93 (53$SiO_2$-6$Na_2O$-12$K_2O$-5MgO-20CaO-4$P_2O_5$ wt%) [26], show reduced tendency to crystallise and are therefore easier to process. To be able to form bioactive glass fibres into textiles, they should be as thin as the technical glass fibres (4–20 µm) and must have sufficient tensile strength, which, for example, is quoted as about 2000 MPa for unsized and between 2500 to 4000 MPa for sized E-glass fibres [21,27].

A wide variety of diameters for continuous fibres made from bioactive glasses have been reported in the literature. Mishra et al. produced core-clad fibres from phosphate glass with diameters of 110 µm and 140 µm [28]. Even larger sizes were reported by Pirhonen, who fabricated silicate glass fibres from 13-93 glasses and coated them with various polymers. The average thicknesses were consistently above 200 µm [29]. These fibres degrade slowly over a long period of time, but are most likely not suitable for textile processing due to the large bending stiffness of such thick fibres. Lehtonen et al. showed that thin bioresorbable silicate fibres can also be produced [30]. Three glass compositions were drawn into fibres with an average thickness of 13 µm by melt spinning. Strengths were exceptionally high for the bioactive glasses, with values around 2000 MPa. The dissolution behaviour was studied in Tris buffer and SBF over a period of 26 weeks. All fibre compositions studied by Lehtonen et al. [30] , including the E-glass, showed significant strength loss in SBF after 26 weeks.

In this work, the temperature and viscosity behaviour of four different glass systems (S53P4, 13-93, 1-06 and 18-06), whose composition was already reported by Vedel et al. [31,32], were investigated and evaluated regarding their fibre spinnability. The glasses investigated were chosen because of their different compositions and associated properties, such as drawability and bioactivity. Glass S53P4 was chosen despite its comparatively low processing range because this glass is already approved in the form of granules for the repair of bone defects [7] and the production of fibres from this glass would be advantageous for the manufacture of various medical devices. Glass 13-93 was specially developed for the production of fibres starting from glass S53P4. So far, however, it has not been possible to produce fibres with a diameter below 20 µm from this glass [33]. Therefore, it should be investigated whether this is possible. Furthermore, this glass did not show such high bioactivity as the original glass composition S53P4, which is the reason why the experimental glass 1-06 was developed. The composition of glass 1-06 is very similar to the composition of 13-93 only with the difference that the addition of boron oxide should increase the solubility and bioactivity. The fourth glass, 18-06, was chosen because of its high $SiO_2$ content, which promises very good processability and thus also spinning reliability.

Continuous fibres were produced from the suitable compositions in a melt spinning process and their mechanical strengths were determined in the single fibre tensile test. In addition, the dissolution behaviour of the fibres in water and simulated body fluid (SBF) at a temperature of 37 °C was investigated by characterising the surfaces and determining the ions released. The stability during storage and the influence of a surface silane coating on the mechanical strengths of single BG 18-06 fibres are presented. To get a first impression of the biocompatibility of the fibres, a murine pre-osteoblast cell line was seeded on them to evaluate the cell morphology after 7 days of culture.

## 2. Materials and Methods

### *2.1. Glass Production*

The glasses 1-06, 18-06, 13-93 and S53P4 with the composition shown in Table 1 were produced by melt-quenching route.

**Table 1.** Glass compositions.

| | 1-06 wt% | 18-06 wt% | 13-93 wt% | S53P4 wt% |
|---|---|---|---|---|
| **$SiO_2$** | 50.0 | 65.0 | 53.0 | 53.0 |
| **$P_2O_5$** | 4 | 0 | 4.0 | 4.0 |
| **$B_2O_3$** | 0.2 | 1.5 | 0 | 0 |
| **$Na_2O$** | 5.9 | 18.4 | 6.0 | 23.0 |
| **$K_2O$** | 12.0 | 0 | 12.0 | 0 |
| **CaO** | 22.6 | 15.0 | 20.0 | 20.0 |
| **MgO** | 5.3 | 0.1 | 5.0 | 0 |

For the production of the glasses, 150 g of mixture were weighed in and mixed for 30 min in an overhead mixer at a constant speed to homogenize the mixtures. The batch was then filled into platinum crucibles and melted at 1360 °C for 30 min. In order to improve the homogeneity of the glass, the melt was stirred with the help of a corundum rod after the 30 min and was melted for another 5 min. Afterwards the glass was cast out to cuboids and tempered. The raw materials used with the exact quantities can be seen in Table 2.

**Table 2.** Composition of the batches.

| Glass | 1-06 g | 18-06 g | 13-93 g | S53P4 g |
|---|---|---|---|---|
| **Quartz powder** | 60.42 | 78.09 | 65.07 | 61.53 |
| **Calcium carbonate p.A.** | 49.34 | 32.55 | 44.36 | 42.04 |
| **Potassium carbonate p.A.** | 21.28 | 0 | 21.62 | 0 |
| **Sodium orthophosphate p.A.** | 11.18 | 0 | 11.35 | 10.76 |
| **Sodium carbonate p.A.** | 1.19 | 36.74 | 0 | 35.66 |
| **Sodium tetraborate p.A.** | 0.35 | 2.61 | 0 | 0 |
| **Magnesium oxide p.A.** | 6.24 | 0.01 | 5.99 | 0 |
| **Total weight** | 150.00 | 150.00 | 150.00 | 150.00 |

In order to determine the exact composition of the glasses and the deviations from the synthesis composition, glass powder was analysed using Inductively Coupled Plasma Optical Emission Spectrometry (ICP-OES). For this purpose, a small portion of the glass cuboids was crushed and ground with a ball mill Pulverisette 6 (FRITSCH, Idar-Oberstein, Germany) at 350 rpm for a period of 8 min. Subsequently, the glass powder was sieved to a particle size of less than 63 µm using the sieve shaker AS 200 (RETSCH, Haan, Germany). The glass powders were then digested with hydrofluoric acid and perchloric acid and the resulting solution was analysed by ICP-OES Spectro Flame Compact S (SPECTRO, Kleve, Germany).

The values determined for the synthesis, and analytical compositions are shown in Table 3.

This table reveals only very minor differences between the synthesis and analytical compositions of the various glasses that can be attributed to impurities or weighing errors. In addition, there are also measurement errors for this measurement. The measurement errors vary for the different ions and depend on the method used. For the measuring methods used in this case, the measurement error for $P_2O_5$ and $B_2O_3$ is less than $\pm 0.1$. For the sodium and potassium oxide, the error is $\pm 0.2$ and for CaO $\pm 0.3$. For the determination of the concentration of the magnesium ions, the error is $\pm 0.1$. The measurement error for $SiO_2$ is the sum of the single errors and is $\pm 1$.

**Table 3.** Synthesis and analysis composition of the glasses.

| | Synthesis 1-06 wt% | Analysis 1-06 wt% | Synthesis 18-06 wt% | Analysis 18-06 wt% | Synthesis 13-93 wt% | Analysis 13-93 wt% | Synthesis S53P4 wt% | Analysis S53P4 wt% |
|---|---|---|---|---|---|---|---|---|
| **$SiO_2$** | 50.0 | 52.63 | 65.0 | 66.87 | 53.0 | 52.25 | 53.0 | 53.22 |
| **$P_2O_5$** | 4.0 | 4.19 | 0 | 0.48 | 4.0 | 4.07 | 40 | 4.12 |
| **$B_2O_3$** | 0.2 | 0.20 | 1.5 | 1.50 | 0 | 0 | 0 | 0 |
| **$Na_2O$** | 5.9 | 5.56 | 18.4 | 16.47 | 6.0 | 5.46 | 23.0 | 21.48 |
| **$K_2O$** | 12.0 | 11.71 | 0 | 0.04 | 12.0 | 10.88 | 0 | 0.04 |
| **CaO** | 22.6 | 21.87 | 15.0 | 14.44 | 20.0 | 23.13 | 20.0 | 21.04 |
| **MgO** | 5.3 | 3.81 | 0.1 | 0.10 | 5.0 | 4.16 | 0 | 0.04 |

### 2.2. Glass Characterisation

For the production of fibres it is essential to know the processing temperature range as well as the crystallisation and liquidus temperature. These temperatures were determined using a hot stage microscope and a gradient furnace. To determine the processing range, the difference between the spherical and hemispherical temperature is crucial [34]. A hot stage microscope was used for this purpose. A glass powder was produced from the previously manufactured glass cuboids. From this powder, a sample cylinder with a diameter of 3 mm and a height of 3 mm was produced, which was placed on a platinum plate and heated in the hot stage microscope to a temperature of 1300 °C with a heating rate of 10 K/min. The surface temperature curve, as well as the softening, spherical and hemispherical temperatures were recorded. These temperatures represent specific viscosity fixed points and can be determined via the sample geometry. The following values characterise the viscosity points: $10^{6.1}$ Pa·s: spherical temperature; $10^{4.5}$ Pa·s: hemispherical temperature and $10^{4.2}$ Pa·s: flow temperature. These viscosity fixed points were determined by Scholze [34]. For further processing, the difference between the spherical and hemispherical temperature is of decisive importance, as this indicates the processing range.

A gradient oven was used to determine the liquidus temperature. For this purpose, glass rods were produced, which were left on a platinum boat in a furnace with a defined temperature profile for two hours. Afterwards, the start of crystallisation was determined with the digital microscope Keyence VHX700 (Keyence, Neu-Isenburg, Germany). With the help of the known temperature profile, the liquidus temperature could be calculated.

### 2.3. Glass Fibre Production

The fibres were produced using the down drawing process. A schematic representation of the drawing equipment can be seen in Figure 1.

A platinum crucible with 8 nozzles with a diameter of 2.5 mm was used. The temperature near the tips and in the crucible was adjusted and monitored using two pyrometers. The fibre diameter was adjusted to between 15 and 17 µm by the fine tuning crucible temperature and the winder speed. During the first drawing tests, the previously cast glass block was heated with the crucible, which led to increased crystallisation. To prevent this, the platinum crucible was heated up to the target temperature without glass, then the glass was added and melted.

First, fibres were drawn from glass 18-06. The crucible temperature was 1200 °C and the temperature at the nozzles was 1110 °C. The desired fibre diameter of 14.9 µm was achieved at a drawing speed of 1413 m/min. During the drawing of the fibres no drawing bulbs were formed, but drops from which the fibres were drawn. The formation of crystals during the drawing process was detected in these glass fibres. These crystals are formed by heterogeneous nucleation, reducing the tensile strength of the glass fibres and increasing the risk of fibre breakage. For glass 1-06, the crucible temperature was 1270 °C and the nozzle temperature was 1170 °C. At these temperatures, it was possible to draw fibres with 15.1 µm at drawing speed of 1413 m/min without breakage. Surface crystallisation also

occurred in this glass. In addition, segregation of the fibres during the drawing process was observed. Many trials were required to produce fibres from glass 13-93, as this glass exhibited an increased tendency to crystallise. As a result, the fibres kept breaking off during the drawing process. At a crucible temperature of 1220 °C and a nozzle temperature of 1120 °C, fibres with a diameter of 15.5 µm could be produced at a drawing speed of 848 m/min. There were many difficulties in producing fibres from the glass S53P4. Because of the very high tendency to crystallise, which was already observed during the production of the preform. Additionally, the narrow processing temperature ranged between 1050 and 1075 °C, lowering the drawability of the glass fibres, so the spinning tests were aborted. The drawing parameters and achieved fibre diameters are summarized in Table 4.

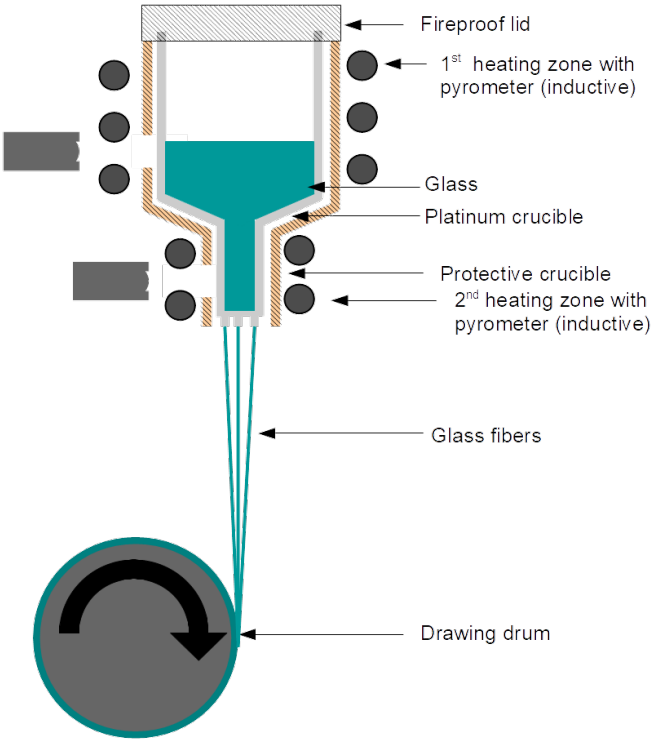


**Figure 1.** Schematic illustration of the fibre drawing plant.

**Table 4.** Drawing parameters of the produced fibres.

| Glass | Crucible Temperature °C | Nozzle Temperature °C | Drawing Speed m/min | Fibre Diameter µm |
|---|---|---|---|---|
| **1-06** | 1270 | 1170 | 1413 | 15.3± 1.3 |
| **18-06** | 1200 | 1110 | 1413 | 14.9 ± 1.5 |
| **13-93** | 1220 | 1120 | 848 | 15.5 ± 2.1 |

### *2.4. Single-Fibre Tensile Test (SFTT)*

The tensile strength of single fibres after drawing, storing and silanisation was conducted in accordance to DIN EN ISO 5079 by using the Favimat+ (Textechno, Germany) automatic single-fibre test system. The fibres to be tested were stored at a standard climate for at least one hour before the measurement. The fibres were then separated with the help of a dissecting needle and a pretension weight with a mass of 150 mg was applied. Single fibres were fixed between two clamps with a gauge length of 50 mm. Before the tensile test, the diameter of the single filament can be determined by the vibroscopic method, in which the fibre is set in vibration and its resonance is registered by an optoelectric sensor.

The tensile test was performed at room temperature and a speed of 25 mm/min. A total of approximately 50 fibres were tested and the results are presented as mean value with standard deviation. Due to the brittle nature of the fibres, the Weibull statistic was used to describe the reliability of the strengths. The Weibull modulus (m) is not a material constant, but it gives a good indication of how homogeneous the material is. The Weibull modulus can therefore be considered as a defect frequency distribution factor. High values (>4) indicate that defects are evenly distributed in the material, whether they are plentiful or not, so the strength is almost independent of the length of the fibres. Low values indicate that the flaws are less evenly distributed. This leads to a greater scatter in the strength. The Weibull modulus is therefore a tool for evaluating the homogeneity of the fibre in terms of mechanical properties. The two-parameter Weibull distribution describes the probability of failure $P$ by:

$$P = 1 - e^{-\left(\frac{\sigma}{\sigma_c}\right)^m} \quad (1)$$

where $m$ is the Weibull modulus, $\sigma_0$ is the scale parameter (Weibull critical strength), and $\sigma$—the fracture strength. The characteristic strength $\sigma_0$ is slightly higher than the average strength and corresponds to the value of the stress for which the probability of failure ($P$) is equal to 63.2 % [30,35]. Figure 2 displays the Weibull assessment exemplarily for glass 18-06.

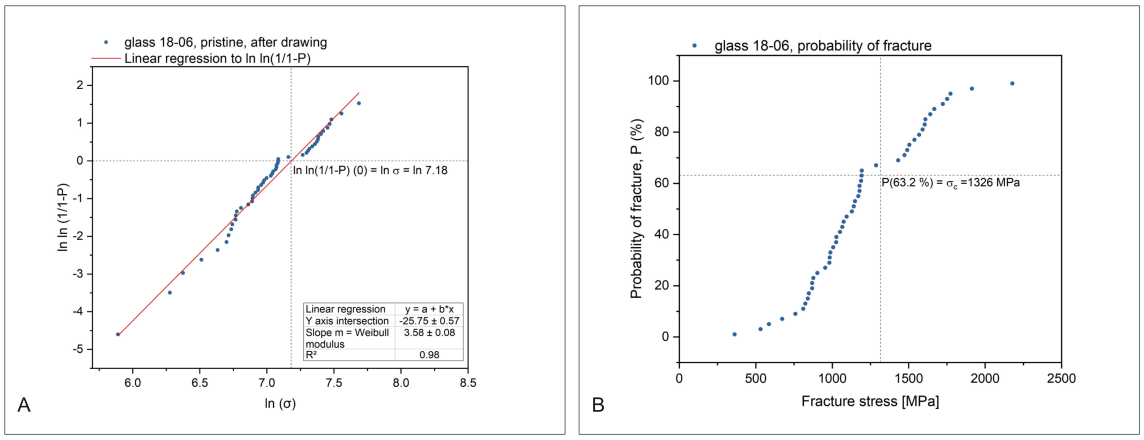


**Figure 2.** (**A**) Weibull statistics, the Weibull modulus (slope of the regression line) was determined as 3.58; (**B**) Plot of the probability of fracture P against the fracture stress [MPa].

### *2.5. Glass Fibre Silanisation*

Organofunctional silanes fill surface flaws and thus improve the fibre strength. Moreover the silanes act as adhesion promoter between the glass surface and polymers in composites. The following organofunctional silanes, purchased from Evonik Industries AG (Germany), have been applied to BG 18-06 fibres: 3-Glycidoxypropyltrimethoxysilane (GTPMS, Dynasylan® GLYMO), 3-Aminopropyltriethoxysilane (APTES, Dynasylan® AMEO), Propyltrimethoxysilane (Dynasylan® PTMO) and N-2-Aminoethyl-3-aminopropyltrimethoxysilane (Dynasylan® DAMO). Aqueous solutions of a concentration of 2.0 wt% were prepared from each silane.

The glass fibres were carefully clamped onto a frame, which was then immersed in the silane solution using a dipping machine at a speed of 80 mm/min. After one minute of immersion, the frame was removed, air dried for 30 min and then dried at 120 °C for 30 min.

### *2.6. Degradation Studies and Storage*

In order to determine the dissolution of the produced glass fibres and the associated property changes, they were stored in SBF [36]. The composition and pH value of this fluid is comparable to the inorganic portion of human blood plasma and was prepared according

to Kokubo. For the storage experiments 10–15 fibres with a length of 10 cm were separated and grouped into bundles. These fibre bundles were wrapped around a titanium wire and inserted into the 50 mL sample tubes made of scratch-free plastic. The titanium wire was used to facilitate handling of the fibres. The tubes were filled with deionized water or SBF and stored at 37 °C for different time periods in a drying oven. The temperature of 37 °C and the pH value of the SBF of 7.4 were chosen because these are physiological conditions of living organisms. Initially, the fibres were stored for 1, 2, 4, 6 and 8 weeks. Due to the high bioactivity and associated dissolution of the fibres made by glass 1-06 and 13-93, the storage times for these glasses were shortened to 1, 2, 4 and 5 days and 1, 2, 4 and 6 hours, respectively. After storage, the pH value of the SBF solution was determined and the fibres were removed, thoroughly rinsed with deionized water, and dried in the drying oven at 50 °C for 16 h. The liquid in the tubes was filtered and its composition was analysed using ICP-OES. The glass eluate method was applied using water as the matrix. Additionally, topographic images were takes with a scanning electron microscope (SEM, ULTRA PLUS, Zeiss, Oberkochen, Germany) to observe the dissolution behaviour and resulting changes of the fibre surface structure.

To investigate the effect of storage, glass 18-06 was stored in a desiccator over silica beads and the strength of the fibres was determined after 8 and 16 months.

### 2.7. Cell Culture

Murine calvarial pre-osteoblast cell line MC3T3E1 subclone 4 (CRL-2593) was purchased from ATCC (Manassas, VA, USA) and cultured in alpha modified minimum essential medium with nucleosides (M4526, Sigma-Aldrich), supplemented with 10 % $v/v$ FBS, 1 % $v/v$ P/S and 1 % $v/v$ GlutaMAX (35050, Gibco®). Culture was performed at 37 °C with 5 % $CO_2$ and 100 % humidity. Medium was refreshed twice per week and cells were expanded before reaching confluency. Experiments were performed at passages 19–22. The BG fibres were sterilised at 220 °C for 2 h, after which the fibres consequently weighted in the desired amounts to reach final concentrations of 10 mg/ml.

Cells were seeded at a concentration of 3500 cells/cm$^2$ in the wells of an optical 24-well plate where bioactive glass was previously placed to reach concentration 10 mg/mL. The cells were incubated for 7 days and fixated with 4 % paraformaldehyde (PFA). Fixation reaction was quenched with 25 mM $NH_4Cl$ in PBS for 1 h. Immunofluorescent stainings were performed against fibronectin (primary antibody: anti-fibronectin antibody, ab23750, Abcam plc. Secondary antibody: Alexa Fluor 488, A-21206, Invitrogen), actin filaments (Phalloidin Atto 550, 19083, Sigma-Aldrich) and nuclei (DRAQ5, 62251, Thermo Scientific). Image stacks were recorded with a Leica SP5 II confocal laser microscope equipped with a MaiTai HP multiphoton laser (Mai Tai HP®, Spectra Physics) with two photon excitation at 910 nm and signal detection at 450–460 nm to visualise fibrillar collagen type I and 25× water immersion objective.

## 3. Results

### 3.1. Glass Melting Properties

The temperature-dependent surface curves detected with the hot stage microscope are shown in Figure 3.

A closer look at the curves reveals a slight increase in surface area for all glasses up to approx. 600 °C, which can be attributed to thermal expansion. After that, all glasses showed a rapid reduction in surface area with increasing temperature. Softening and the corresponding softening temperature were detected in this area. The further slower reduction of the area was caused by the melting of the sample and the formation of the spherical shape. As the temperature increased, a noticeable increase in surface area was detected in all glasses. After a correspondingly high temperature was reached, the previously formed crystals dissolved and the hemispherical geometry was achieved. This was associated with a further decrease in surface area. Subsequently, at a sufficiently high temperature, the glass started to flow. Glass S53P4 is an exception. This glass already

crystallised before reaching the softening temperature, which can be clearly seen from the small change in the surface area between 630 °C and 850 °C. After a correspondingly high temperature led to the dissolution of the crystals, softening, spherical and hemispherical temperatures with small temperature differences were recorded. Table 5 shows the typical sample shapes corresponding to the fixed viscosity points for the glass 18-06.

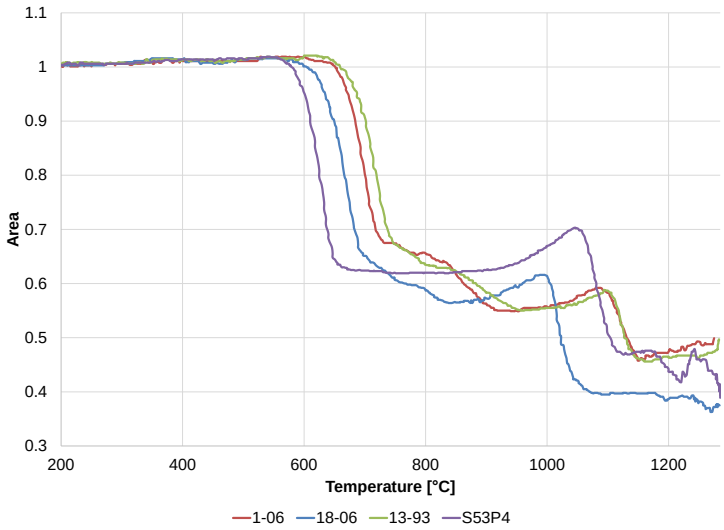


**Figure 3.** Temperature-dependent surface curve in the hot stage microscope.

**Table 5.** Sample shapes for Glass 18-06 during heating in the hot stage microscope.

| | Begin | Softening Point | Spherical Point | Hemispherical Point | End |
|---|---|---|---|---|---|
| |  | 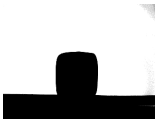 | 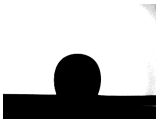 |  |  |
| **Temperature [°C]** | RT | 763 | 807 | 1013 | 1250 |
| **Viscosity [dPa·s]** | - | $10^{8.2}$ | $10^{6.1}$ | $10^{4.5}$ | $10^{4.2}$ |

The temperatures determined with the hot stage microscope and gradient oven are listed in Table 6.

**Table 6.** Results from heating microscope and gradient furnace.

| Glass | 1-06 | 18-06 | 13-93 | S53P4 |
|---|---|---|---|---|
| **Softening temperature [°C]** | 759 | 763 | 820 | 1020 |
| **Spherical temperature [°C]** | 836 | 807 | 864 | 1053 |
| **Hemispherical temperature [°C]** | 1096 | 1013 | 1111 | 1078 |
| **Processing range [K]** | 260 | 206 | 247 | 25 |
| **Liquidus temperature [°C]** | 1142 | 1023 | 1168 | 1141 |

Glass 18-06 has the lowest liquidus temperature, while the glass 13-93 has the highest. Comparable liquidus temperatures were determined for the glasses 1-06 and S53P4. The widest processing range was determined for glass 1-06 and the narrowest for glass S53P4. Based on these results, glass 18-06 should have the best drawing properties while glass S53P4 should not be drawable to fibres. The production of fibres from the other two glasses 13-93 and 1-06 should also be possible.

### *3.2. Mechanical Properties of the Bioactive Glass Fibres*

The glasses 1-06, 13-93 and 18-06 were successfully drawn into continuous fibres. For use in load-bearing implants, the mechanical strength is crucial. In Table 7, the average tensile, Weibull critical strength, Weibull modulus and fibre diameter are presented.

The glass fibres of glass 1-06 showed the highest tensile strengths with the largest standard deviation. The large standard deviations and small strength values of the measured fibres are due to the formation of crystals during the drawing process of the fibres.

**Table 7.** Strength values of bioactive glasses with standard deviation.

| Glass | Tensile Fracture Strength MPa | Weibull Critical Strength $\sigma_0$ MPa | Weibull Modulus $m$ | Fibre Diameter µm |
|---|---|---|---|---|
| **1-06** | 1261 ± 473 | 1432 | 2.6 | 12.0 ± 1.4 |
| **18-06** | 1185 ± 382 | 1316 | 3.6 | 13.7 ± 1.0 |
| **13-93** | 877 ± 310 | 977 | 3.4 | 11.8 ± 1.1 |

### *3.3. Glass Degradation and Storage*

#### 3.3.1. Determination of the pH Value Curve

After storage, the pH values of the SBF solutions were measured. The values obtained can be seen in Figure 4.

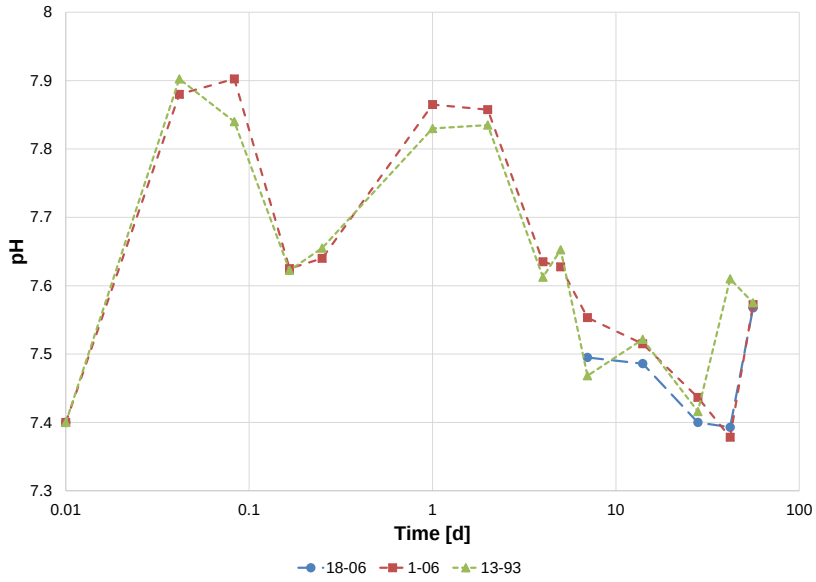


**Figure 4.** Changes of the pH value of the SBF solution at 37 °C.

From Figure 4 it can be seen that the pH value for the fibres of glasses 1-06 and 13-93 increase very rapidly from the previously set value of 7.4 to a value of 7.9 within the first hours of dissolution. This can be explained by the exchange between the $Ca^{2+}$ and $Na^{+}$ ions in the material and the $H^{+}$ and $H_3O^{+}$ ions from the environment and the formation of silanol compounds on the surface, which increased the pH value of the solution. Afterwards, the pH value dropped and rose again after one day. This can be explained by the formation of an unreacted fibre surface, which led to a repetition of the initial reactions of the dissolution. This process was observed again until days 42 and 56, respectively. Consequently, the process is a cyclic one. The fibres decompose on the surface and release fresh, unreacted material after the reaction layer is removed. Consequently, the formation of a hydrated surface layer initially leads to an increasing pH value. It decreases when the surface layer has completely dissolved. The pH value of the SBF solution of 18-06 increases to 7.5 within the first week, after which the pH value of the solution decreases again and reaches its

maximum at 7.57 after 56 days of storage. The final increase for all three glass fibres can be explained by a sediment reaction.

### 3.3.2. Determination of the Ion Concentration

In addition to the pH values, the ion concentrations of the solutions were also determined by ICP-OES. In case of SBF determining the change of Si-Ions-concentration over time was possible. For the other ions was it impossible to measure the concentrations, as the SBF includes many different salts.

The concentration of $Si^{4+}$ ions as a function of time can be seen in Figure 5 and increased for all glasses as the dissolution time progresses. Glass 1-06 showed the highest $Si^{4+}$ concentration of all glasses after 14 days. Thereafter, the concentration of $Si^{4+}$ ions decreased sharply. Glass 13-93 also showed a maximum after 14 days with a subsequent decrease in concentration. At this point, the fibres of these two glasses were almost completely dissolved. This suggests the formation of a precipitate in the form of poorly soluble compounds in both glasses. For glass 18-06, the maximum $Si^{4+}$ ion concentration was determined after a storage period of 28 days. From this point on, a precipitate could be seen at the bottom of the tubes used to store the fibres.

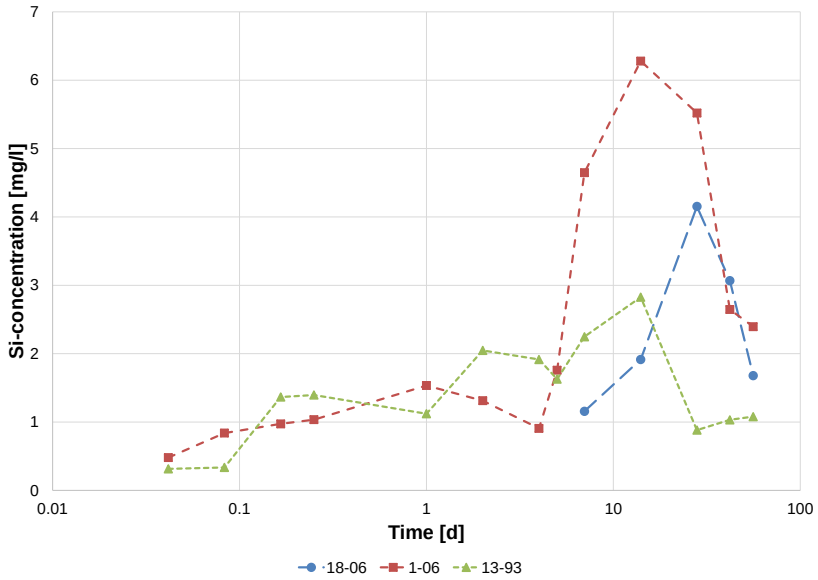


**Figure 5.** Concentration of silicon ions in SBF in relation to time.

By analysing the deionized water, the concentration of silicon, potassium, calcium and magnesium ions could be measured. For glass 18-06, the concentration of the various ions as a function of storage time is shown in Figure 6.

The silicon content dropped to a minimum after 28 days of storage. The concentration of calcium ions also decreased at this time. Thereafter, the concentration of $Si^{4+}$ and $Ca^{2+}$ ions increased again and reached another minimum after 56 days. These results were not expected, as the glass fibres should simply dissolve during storage and the concentration of the various ions should slowly increase. A possible explanation for the low measured values is the formation of poorly soluble compounds. Glass 18-06 contains very little magnesium (cf. Table 3) and the contents dissolved in the water are below the detection limit.

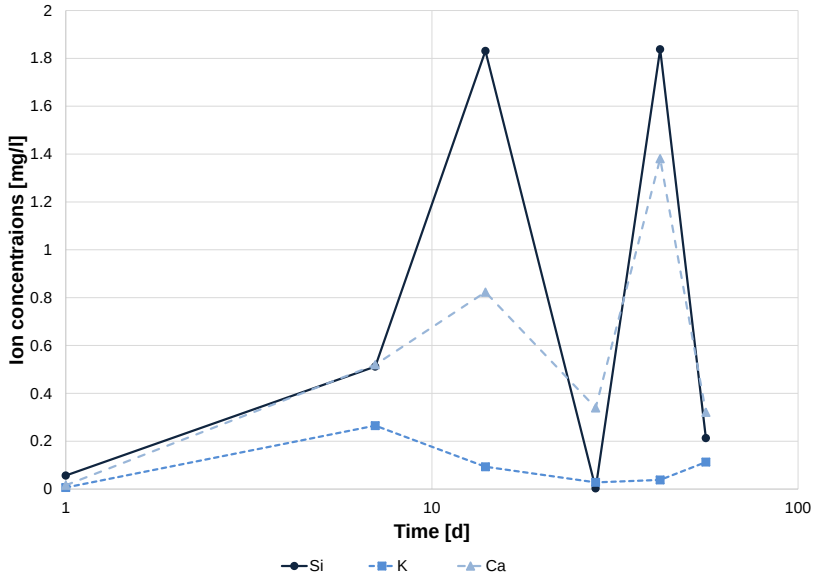


**Figure 6.** Ion concentration in deionised $H_2O$ in relation to time for glass 18-06.

The concentration of the different ions for glass 1-06 in dependence of the storage time can be seen in Figure 7.

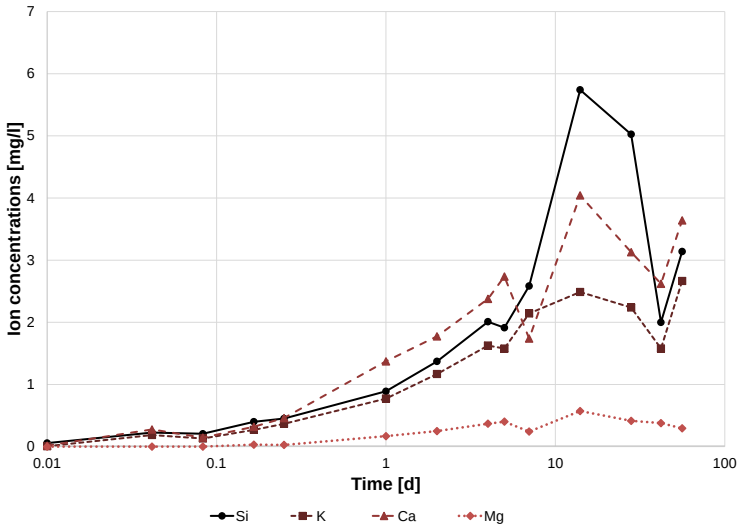


**Figure 7.** Ion concentration in deionised $H_2O$ in relation to time for glass 1-06.

The concentration of silicon ions increased up to a maximum at a storage period of 14 days. Thereafter, the $Si^{4+}$ ion concentration decreased again. The $Ca^{2+}$ and $K^+$ ion concentrations also increased up to the storage period of 14 days and then decreased again. The reduction of the ion concentrations can also be attributed here to the formation of poorly soluble compounds. Only the concentration of magnesium ions increased very slowly and continuously.

Figure 8 shows the concentration of the various ions as a function of the storage time for glass 13-93.

The concentration of silicon ions increased as the storage period progresses and reached a maximum after 14 days. After that, the concentration dropped sharply again. The concentration of calcium ions also increased and reached a maximum after 2 days. Thereafter, the ion concentration decreased. The concentration of potassium ions increased and slowly decreased after 4 days. Furthermore, the concentration of magnesium ions increased slowly and decreased slowly after 2 days. The increase in ion concentrations

can be explained by the complete dissolution of the fibres after 2 days and the associated release of ions. The further increase in ion concentrations of silicon and calcium ions can be attributed to minimal remnants of undissolved fibres, which were no longer visible to the naked eye and were filtered off prior to analysis of the eluates. The decrease may be due to the formation of poorly soluble salts.

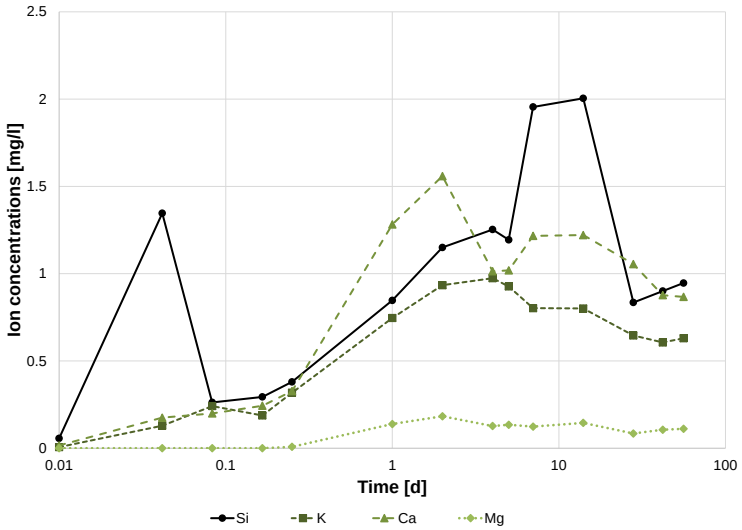


**Figure 8.** Ion concentration in deionised $H_2O$ in relation to time for glass 13-93.

3.3.3. Examination of the Fibres with SEM

In order to be able to determine the reactions at the fibre surface during dissolution more precisely, SEM examinations were carried out. Due to the large sample size and time required, the fibres of all glasses stored in water and SBF were only prepared and observed at the first three sampling times. The surface and the cross-section of the fibres were examined.

Figure 9 shows the unreacted fibres. All fibres feature light and dark areas and bumps on the fibre surface, which indicates segregation and the formation of crystals during the drawing process.

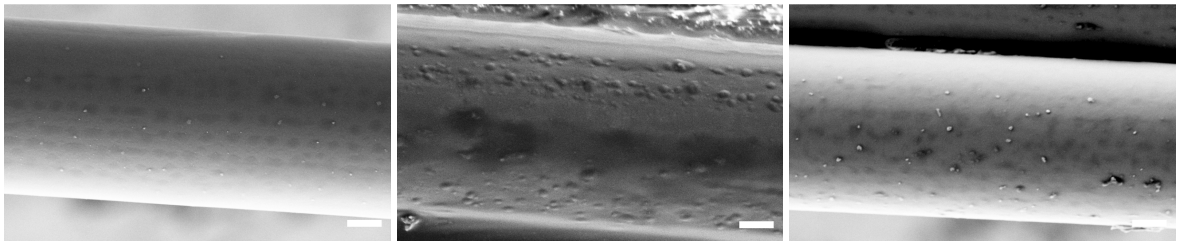

(a) 1-06 (b) 18-06 (c) 13-93

**Figure 9.** SEM images of the unreacted fibres (scale bars 2 µm).

The dissolution of the fibres of glass 18-06 in deionised water and SBF is shown comparatively in Table 8.

In the case of the fibres stored in water, it can be seen that after 7 days the surface of the fibre was slightly roughened. After longer storage, no unevenness could be detected on the surface. This is due to the formation of an outer corrosion layer, which has been dissolved as the storage time progressed. The fibres stored in SBF showed a rough surface with irregular dissolution after a storage period of 7 days. Even after 14 days, an uneven dissolution of the fibre could be observed. This is due to segregation across the fibre cross-section, which occurred during the drawing process. Furthermore, the roughness

of the fibre surface increased with increasing storage time and the diameter of the fibres decreased. Which surface reactions have taken place and which layer might have been deposited on the surface must be clarified in further investigations.

**Table 8.** SEM images of the dissolution of the fibres of the glass 18-06 (scale bars 2 µm).

| Time | 7 Days | 14 Days | 28 Days |
|---|---|---|---|
| $H_2O$ | 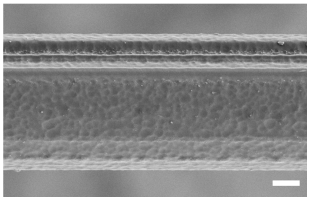 | 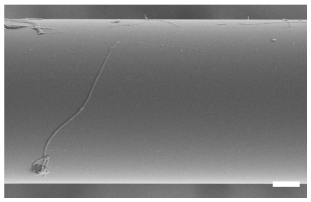 | 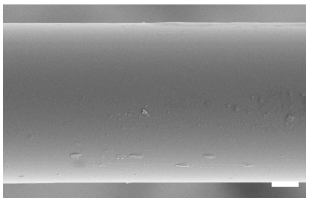 |
| SBF | 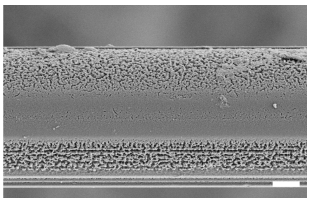 | 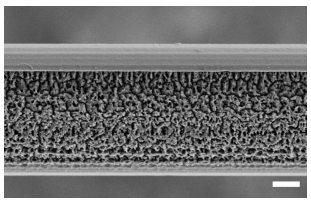 | 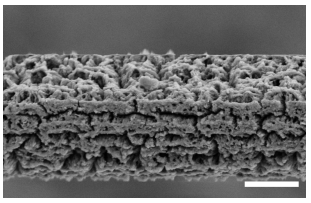 |

Table 9 shows the dissolution of the fibres of glass 1-06 in the two solutions. Since the fibres dissolved very quickly in SBF, only the fibres after a storage period of one and two hours could be observed.

**Table 9.** SEM images of the dissolution of the fibres of the glass 1-06 (scale: 2 µm).

| Time | 1 h | 2 h | 4 h |
|---|---|---|---|
| $H_2O$ | 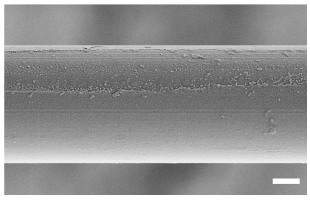 | 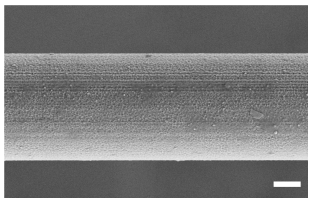 | 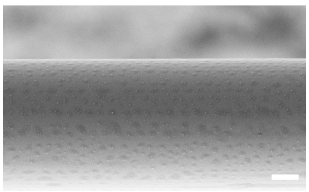 |
| SBF | 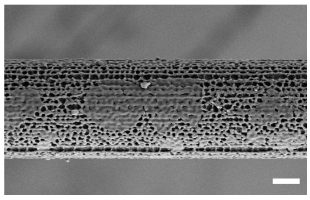 | 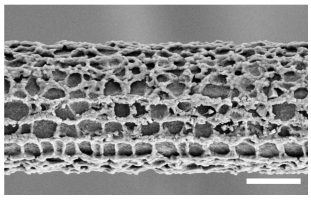 | |

After storing the fibres in deionised water for one hour, an incomplete layer could be seen on the surface of the fibres. After two hours of storage, a roughened fibre surface was formed. This indicates the dissolution of the layer, which can already be observed after one hour. During further storage, the rough surface layer reacted with the surrounding medium and a smooth fibre surface was formed. The fibres stored in SBF already exhibited a very roughened surface after only one hour, which further reacted with increasing storage time to form a skeletal surface. The more strongly roughened areas of the fibres correspond to the dark areas that can be seen in the original fibres (cf. Figure 9a). These areas have a different composition due to the segregation and dissolve more easily (see SEM image after 2 h in SBF in Table 9). The diameter of the fibre decreased during storage in both media.

The images of the glass fibres with composition 13-93 with increasing storage time and dissolution are shown in Table 10.

In the case of fibres stored in deionised water, a slightly roughened surface layer formed after 1 h of storage, which dissolved again with increasing storage time. The fibre

diameter considerably dropped after four hours. The fibres stored in SBF showed an incompletely reacted rough surface after one hour, which continued to react as storage progressed. After two hours, larger bumps were visible on the fibre. These are probably crystals. The diameters of the fibres decreased sharply, especially after 4 h of storage. At this time, a very strong reaction of the fibres with the surrounding medium could be observed, forming a very rough and uneven layer. The cause of this irregular reaction is the segregation of the fibres during production.

**Table 10.** SEM images of the dissolution of the fibres of the glass 13-93 (scale bars 2 µm).

| Time | 1 h | 2 h | 4 h |
|---|---|---|---|
| $H_2O$ | 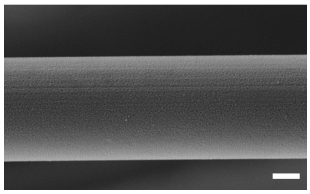 | 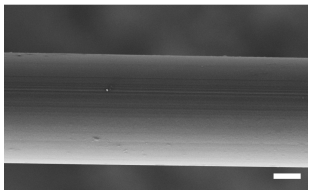 | |
| SBF | 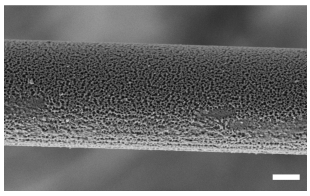 | 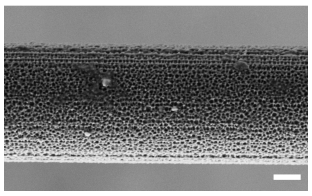 | 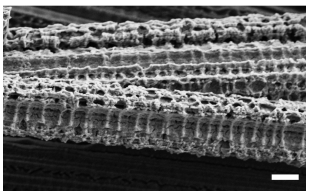 |

Furthermore, the cross-sectional areas of the fibres were also examined. The image of the fractured surface of a fibre of glass 18-06 can be seen in Figure 10. What can be clearly observed is that the fracture surface is very irregular, which does not correspond to the appearance of a typical glass fracture surface. The formation of crystals during the drawing process redirects the crack energy. The crystals are clearly visible.

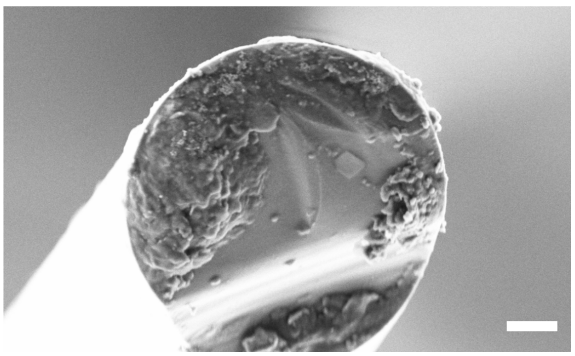

**Figure 10.** SEM images of the fibre cross-sections of 18-06 (scale bar 2 µm).

It is also worth observing the dissolution of different areas at various rates. This is due to the segregation of the glass over the length of the fibres during the drawing process. A SEM image of such a different dissolution is shown in Figure 11.

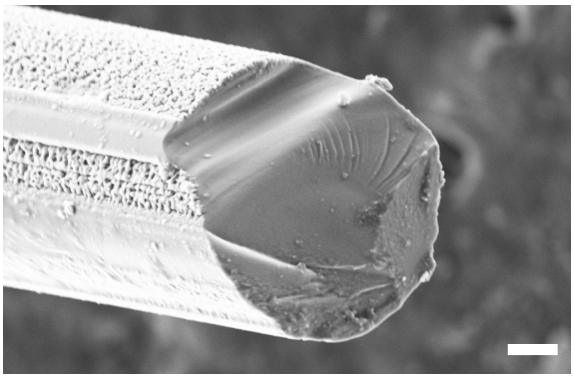

**Figure 11.** Fibre cross-section of glass 18-06 after 14 days storage in SBF (scale bar 2 µm).

#### 3.3.4. Storage of the Fibres

Storage has an influence on the strength of the fibres. The previous results regarding the dissolution of fibres in aqueous solutions suggest that the the fibres may also react with ambient humidity. BG 18-06 fibres were kept in a desiccator for 16 months. Although the storage took place over silica beads, a decrease in strength over time could be observed (cf. Figure 12).

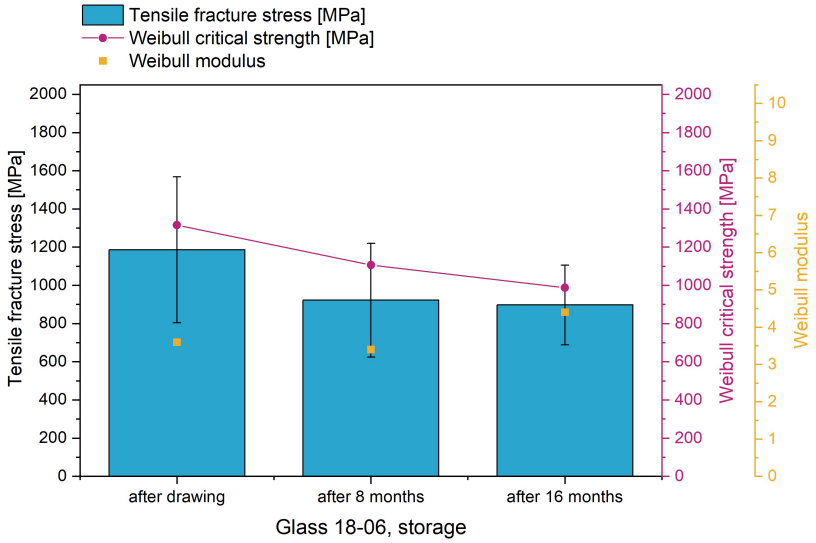


**Figure 12.** Decrease of the tensile strength of glass 18-06 during storage in a desiccator.

### *3.4. Effect of Silanes*

Sizing agents are indispensable for textile fibres. These aqueous solutions often consist of up to 20 individual components. The most important chemical is the organofunctional silane, which acts as a coupling agent due to functional groups that bond with both organic and inorganic materials. The silane is selected according to the organic component, i.e., so that reactive group can effectively bind to, for example, a polymer via the vinyl, amino or epoxy group of the silane. In water, it is first hydrolysed to silanol. When such aqueous solutions are applied to glasses, the unstable silanol condenses into a siloxane/poly(siloxane) network, which is then partially covalently bonded to the glass fibre surface [22]. Since the polysiloxane network is able to bridge small flaws in the glassy structure, the silanes lead to an increase in the strength. This effect was also clearly shown in the present study (Figure 13).

The most stable glass, 18-06, was selected for initial silane coating tests. These fibres, after being stored dry in a desiccator for 8 months, were treated with four silanes commonly used in the industry: 3-Glycidoxypropyltrimethoxysilane (GTPMS, Dynasylan® GLYMO), 3-Aminopropyltriethoxysilane (APTES, Dynasylan® AMEO), Propyltrimethoxysilane

(Dynasylan® PTMO) and N-2-Aminoethyl-3-aminopropyltrimethoxysilane (Dynasylan® DAMO). The silanes improved the strength from an initial value of 922 MPa to values between 1062 MPa and 1203 MPa. This corresponds to a strength increase of 15–30 %. Due to the observed variations, the differences in the average strength values determined for the individual silanes are not significant.

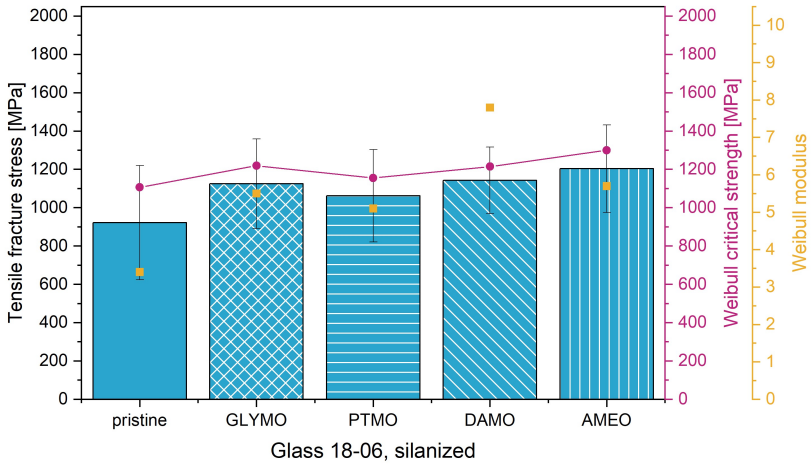


**Figure 13.** Effect of silanes on the tensile strength of glass fibres from glass 18-06.

The silanes also significantly increased the Weibull modulus from 3.4 to over 5. The higher Weibull modulus implies that the defects in the glass surface should now be more uniformly distributed in addition to the mechanical properties of the bioactive glass fibres being more reproducible. While the Weibull modulus for GLYMO (GTPMS), PTMO and AMEO (APTES) were at the same level of about 5.5, the modulus of 7.8 after treatment with DAMO is considerably higher. DAMO is a bifunctional organosilane that, like all other silanes applied in the study, has three hydrolysable inorganic silicon-functional methoxy groups. They react with water under hydrolysis and cleavage of methanol to form the corresponding silanols, which can be bound to the inorganic glass surface. In contrast to the other three silanes, DAMO has an organophilic diamino group. The reason why the binding to the glass surface of DAMO is apparently most effective for 18-06 glass requires clarification in further studies.

### *3.5. Cell–Biomaterial Interaction*

To get a first impression of the biocompatibility of the soluble glasses, fibres of each of the three glass compositions were seeded with osteoblast precursor cells and the cell morphology was assessed microscopically after immunofluorescence staining after seven days (cf. Figure 14). Since bioactive glasses are ideally suited to regenerate bone, a pre-osteoblast cell line was selected. The nuclei (blue), the structural protein actin (magenta) and fibronectin (green) as glycoprotein of the extracellular matrix have been made visible. Actin is one of the most abundant proteins in cells. The protein can be easily labelled with a fluorophore (F-actin), revealing the overall shape and structure of the cell. Fibronectin (FBN) is part of the extracellular matrix (ECM) that, through binding integrin receptors of the cell surface, is a key player of cell behaviour.

Confocal microscopy images showed favourable cell–biomaterial interactions. The cells adhered to all three glass surfaces and wrapped around the individual fibres, depositing the FBN in their vicinity. All three glass compositions allowed the cells to attach well, although it appeared that the pre-osteoblasts adopted the glass fibres as a guide structure, as they aligned themselves precisely along them. No fibrillar collagen type I was observed after 7 days, and no degradation of glass fibres was observed with any of the compositions. From these preliminary results, no visible differences in cell–biomaterial interaction could

be detected and all three bioactive glasses seem to offer a suitable surface for cell adhesion and the secretion of FBN.

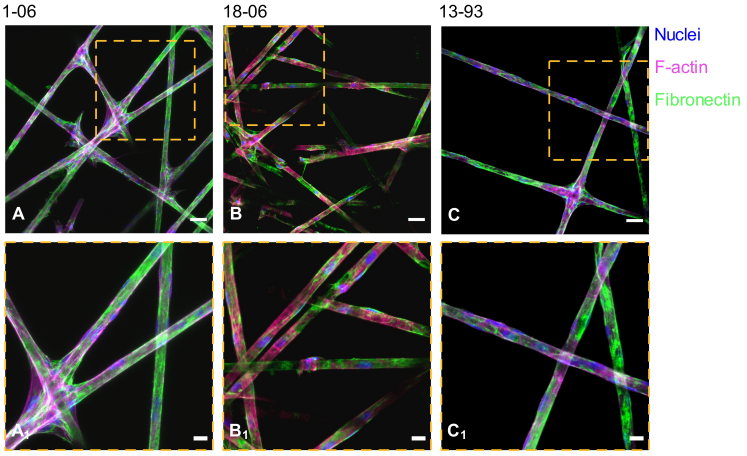


**Figure 14.** Representative images of the pre-osteoblast cells MC3T3-E1 adhered to the distinct bioactive glass fibres (**A**–**C**), depicting nuclei (blue), the structural protein actin (magenta) and the glycoprotein of the ECM fibronectin (green). (**$A_1$**–**$C_1$**) show enlarged sections of the image (magnification in the dashed orange squares). Scale bars 50 µm (**upper row**) and 20 µm (**lower row**).

## 4. Discussion

The production of continuous fibres from medically approved bioactive glasses would be very attractive for many applications. A broad field of application would arise for resorbable materials. Currently, these materials, mostly plastics or metals, are not suitable for load-bearing implants because resorption is inherently accompanied by a loss of mechanical strength. In this regard, fibre-reinforced composites would be of great interest if the degradation of fibres and matrix could be tailored. A suggested concept for resorbable polymers reinforced with bioactive glass fibres for medical applications was presented in the publication by Plyusnin et al. [19]. In this regard, fibres made from hydrolytically active glass compositions could make an important contribution.

In this study, the temperature and viscosity behaviour of the four glass compositions 1-06, 18-06, 13-93 and S53P4 were investigated with regard to the production of continuous fibres. For this purpose, glass cuboids were prepared and the analytical compositions determined.

Various known compositions [31,32] were used to select the glasses and the following considerations were made. S53P4 is a certified bioactive glass, so fibres from these glasses would be of particular interest. It is known from the literature that glass 13-93 can be drawn into fibres [29,37]. Composition 1-06 differs only slightly from this, but in theory should dissolve more quickly because it contains $B_2O_3$. Glass 18-06 is a known experimental composition that has a higher silicate content and is therefore most likely to be processed into fibres.

While glasses 13-93, 1-06 and 18-06 all showed a temperature interval for processing of more than 200 K, for glass S53P4 only a range of 25 K was determined. This is clearly below the 70 K required by Teschner [20] and indicates a very high tendency to crystallise, which could already be demonstrated in the hot stage microscope. It became obvious that glass S53P4 crystallised before reaching the softening temperature. In this respect, it seems almost impossible to produce fibres from this glass composition. With the help of these determined parameters, the fibres for all glass compositions except S53P4 were drawn from previously produced glass blocks using the nozzle drawing method and fibres of diameters below 15 µm were obtained. These diameters correspond to technical glass fibres, for which a range of 4 to 20 µm is reported [21].

The strengths of glass fibres may vary enormously, as they depend on the composition. While military fibre optics glass fibres (FOG-M) have very high tensile strengths of

5570 MPa, porous silica fibres produced by leaching E-glass with hydrochloric acid achieve strengths just below 400 MPa. The strengths of the produced bioactive glass fibres are in the range of about 900 to 1200 MPa and are similar to the values of sodium silicate glass fibres and phosphate glass fibres (300 to 1500 MPa) [21,38], but are significantly below technical E-glass fibers, for which values between 2500 and 4000 MPa are reported [21,27]. Since fibre strength is a measure of both internal structure and surface uniformity, surface defects, segregations or small crystallites appear to be more common in hydrolytically active glass fibres. Although the glass fibres that were produced have comparable $SiO_2$ contents to E-glass fibres (53–65 wt% for BG fibres to 50–60 wt% for E-glass fibres), they do not contain $Al_2O_3$, but instead have significantly greater alkali metal oxide contents such as $Na_2O$ and $K_2O$, which are present in E-glass only in small amounts up to a maximum of 2 wt%. In addition, the 1-06 and 13-93 glasses contain $P_2O_5$, which is responsible for high bioactivity, as hydroxyapatite can form on the surface when the glasses dissolve.

Dissolution of the fibres was observed in all glasses. Fibres of glass 18-06 were the most stable and did not dissolve in deionized water or in SBF in the period of 4 weeks. The fibres of glass 1-06 and 13-93, which according to Vedel [32] have a medium bioactivity, were dissolved within a few hours. However, all glass fibres showed that storage at 37 °C in SBF led to an accelerated degradation. In the case of glasses 1-06 and 13-93, the fibres completely dissolved in SBF in less than one day. This result was unexpected, since 13-93 in particular is considered a glass that dissolves more slowly than S53P4 and 45S5 [39]. Pirhonen et al. studied the dissolution of fibres of glass 13-93 SBF even over a period of 40 weeks [40]. The mean strength after fibre drawing was determined to be 1443 MPa by the authors, which was higher than the 877 MPa observed in the present study. However, fibre diameters of 25–160 µm were obtained, which explains their higher initial strengths on the one hand and the very large variation ranges on the other. It should be noted, however, that fibres were still present after 40 weeks.

The fibres of glass 18-06 with the lowest bioactivity showed the slowest dissolution rate. Since this glass does not contain $P_2O_5$, the bioactivity is lower compared to the other glass compositions. Nevertheless, the slow rate of degradation may be an advantage for medical devices. A slow release of ions does not lead to an abrupt change in the local ion composition, and these fibres would be better suited for reinforcing resorbable implants that need to be mechanically stable over a longer period of time. From the results of the study, it is evident that the dissolution capacity of hydrolytically unstable glasses clearly depends on their particular geometry. Therefore, the dissolution behaviour of the produced fibres cannot be compared with bulk materials or powders.

The lower bioactivity for 18-06 reported in the literature also suggests that less formation of an apatite layer and thus a decreased bioactivity is to be expected [32]. Preliminary experiments with the murine pre-osteoblast cell line MC3T3-E1 showed that the cells adhered well to all three types of glass fibres after seven days, appearing to serve as a guide structure for the cells. Remarkably, the glass fibres of all compositions were still present after the observation period. Based on these preliminary results, further studies need to follow to evaluate the biocompatibility of the glasses with different cell types in detail. In addition, the influence of the medium and the amount of solvent on the dissolution behaviour of the glass fibres need to be investigated.

The issue of sizing is of enormous importance for the fibres and closely related to the dissolution behaviour. If textile-processable resorbable fibres are to be obtained, the size is just as important as the manufacture of the fibres themselves. The key functions of sizings are to protect the glass fibres during production and handling, to establish contact between the individual filaments, as well as to enable bonding between the glass fibre and the polymer matrix. It is also widely proven that the silane component of the sizing is able to repair partially surface flaws of the fibres leading to an increased fibre strength [23,41]. Furthermore, such surface modifications can be utilised to protect the fibres against environmental degradation [22]. The complex sizing compositions have so far been developed and used for technical, i.e., non-resorbable fibres and corresponding fibre–

plastic composites. Medical devices from technical E-glass fibres treated with a standard sizing due to the manufacturing and poly(methyl methacrylate) fibre–plastic composites are produced, which are used, for example, as dentures [42] or cranial implants [15]. As these are permanent implants, little attention needs to be paid to the sizing, which accounts for only a very small proportion of the fibres. Completely new requirements arise for bioactive glass fibres, since the fibres are completely degraded and thus release the sizing back into the environment. This demands that all components of the fibre sizing must be biocompatible if no negative effects are to occur. The development of biocompatible coatings should therefore ideally include in vitro studies.

## 5. Conclusions

In this study, various bioactive glass compositions were thermally analysed and examined for their suitability for fibres production. Thin continuous fibres with diameters of less than 15 µm were produced from glass compositions 13-93, 1-06 and 18-06. To the authors' knowledge, this is the first study that reports the fabrication and characterization of bioactive silicate glass fibres with these diameters. The results may help to produce textiles from resorbable glasses, which are of great interest for numerous medical applications.

**Author Contributions:** Conceptualization, investigation, formal analysis, writing—original draft preparation, J.E. and C.E.; methodology, validation, writing—review and editing, M.G.; investigation, formal analysis, writing—review and editing, R.R., A.X.H.M., A.P.S. and H.F.; writing—review and editing, J.K., N.M., L.H. and M.S.; supervision, funding acquisition, writing—review and editing, M.K. and C.S. All authors have read and agreed to the published version of the manuscript.

**Funding:** This research received no external funding.

**Data Availability Statement:** The data presented in this study are available on request from the first author or the corresponding author. The data are not publicly available due to IPR considerations.

**Acknowledgments:** The authors thank Fritzsche for carrying out the ICP-OES measurements and Treppe and Harnisch for their help in preparing the simulated body fluid. Special thanks to Preßler for the SEM studies of the fibres. We would also like to thank Paula Korn, Katharina Schmidt-Bleek and Carsten Rendenbach for the time they spent in very helpful discussions about the in vitro experiments.

**Conflicts of Interest:** The authors declare no conflict of interest.

## References

1. Ediger, M.D.; Angell, C.A.; Nagel, S.R. Supercooled Liquids and Glasses. *J. Phys. Chem.* **1996**, *100*, 13200–13212. [CrossRef]
2. Brauer, D.S. Bioactive Glasses-Structure and Properties. *Angew. Chem. Int. Ed.* **2015**, *54*, 4160–4181. [CrossRef] [PubMed]
3. Hench, L.L.; Clark, D.E. Physical chemistry of glass surfaces. *J. Non-Cryst. Solids* **1978**, *28*, 83–105. [CrossRef]
4. Cailleteau, C.; Angeli, F.; Devreux, F.; Gin, S.; Jestin, J.; Jollivet, P.; Spalla, O. Insight into silicate-glass corrosion mechanisms. *Nat. Mater.* **2008**, *7*, 978–983. [CrossRef] [PubMed]
5. Engelhardt, H.-J.; von Borstel, L.E. The behaviour of sodium silicate solutions (water glass) in the saline environment and their use in salt mining. *Ger. J. Geosci.* **2014**, *165*, 115–122.
6. Nordberg, M.E. Properties of some Vycor-brand glasses. *J. Am. Ceram. Soc.* **1944**, *27*, 299–305. [CrossRef]
7. Baino, F.; Hamzehlou, S.; Kargozar, S. Bioactive Glasses: Where Are We and Where Are We Going? *J. Funct. Biomater.* **2018**, *9*, 25. [CrossRef]
8. Cunha, M.T.; Murça Maria, A.; Nigro, S.; Klautau, G.B.; Salles, M.J.C. In vitro antibacterial activity of bioactive glass S53P4 on multiresistant pathogens causing osteomyelitis and prosthetic joint infection. *BMC Infect. Dis.* **2018**, *18*, 2305. [CrossRef]
9. Fiume, E.; Barberi, J.; Verné, E.; Baino, F. From Parent 45S5 Composition to Scaffold-Assisted Tissue-Healing Therapies. *J. Funct. Biomater.* **2018**, *9*, 24. [CrossRef]
10. Solanki, A.K.; Lali, F.V.; Autefage, H.; Agarwal, S.; Nommeots-Nomm, A.; Metcalfe, A.D.; Stevens, M.M.; Jones J.R. Bioactive glasses and electrospun composites that release cobalt to stimulate the HIF pathway for wound healing applications. *Biomater. Res.* **2021**, *25*, 4457. [CrossRef]
11. Elschner, C.; Korn, P.; Hauptstock, M.; Schulz, M.C.; Range, U.; Jünger, D.; Scheler, D. Assessing agreement between preclinical magnetic resonance imaging and histology: An evaluation of their image qualities and quantitative results. *PLoS ONE* **2017**, *12*, e0179249. [CrossRef]

12. Korn, P.; Hauptstock, M.; Range, U.; Kunert-Keil, C.; Pradel, W.; Lauer, G.; Schulz, M.C. Application of tissue-engineered bone grafts for alveolar cleft osteoplasty in a rodent model. *Clin. Oral Investig.* **2017**, *21*, 2521–2534. [CrossRef]
13. Nommeots-Nomm, A.; Lee, P.D.; Jones, J.R. Direct ink writing of highly bioactive glasses. *J. Eur. Ceram. Soc.* **2018**, *38*, 837–844. [CrossRef]
14. Petretta, M.; Gambardella, A.; Boi, M.; Berni, M.; Cavallo, C.; Marchiori, G.; Maltarello, M.C.; Bellucci, D.; Fini, M.; Baldini, N.; et al. Composite Scaffolds for Bone Tissue Regeneration Based on PCL and Mg-Containing Bioactive Glasses. *Biology* **2021**, *10*, 398. [CrossRef] [PubMed]
15. Vallittu, P.K. Bioactive glass-containing cranial implants: An overview. *J. Mater. Sci.* **2017**, *52*, 8772–8784. [CrossRef]
16. Shah Mohammadi, M.; Ahmed, I.; Muja, N.; Rudd, C.D.; Bureau, M.N.; Nazhat, S.N. Effect of phosphate-based glass fibre surface properties on thermally produced poly(lactic acid) matrix composites. *J. Mater. Sci. Mater. Med.* **2011**, *22*, 2659–2672. [CrossRef]
17. Souza, M.; Tansaz, S.; Zanotto, E.; Boccaccini, A. Bioactive Glass Fiber-Reinforced PGS Matrix Composites for Cartilage Regeneration. *Materials* **2017**, *10*, 83. [CrossRef]
18. Liu, X.; Rahaman, M.N.; Day, D.E.; Bose, S. In Vitro Degradation and Conversion of Melt-Derived Microfibrous Borate (13-93B3) Bioactive Glass Doped with Metal Ions. *J. Am. Ceram. Soc.* **2014**, *97*, 3501–3509. [CrossRef]
19. Plyusnin, A.; He, J.; Elschner, C.; Nakamura, M.; Kulkova, J.; Spickenheuer, A.; Scheffler, C.; Lassila, L.V.J.; Moritz, N. A Polymer for Application as a Matrix Phase in a Concept of In Situ Curable Bioresorbable Bioactive Load-Bearing Continuous Fiber Reinforced Composite Fracture Fixation Plates. *Molecules* **2021**, *26*, 1256. [CrossRef]
20. Teschner, R. *Glasfasern*; Springer: Berlin/Heidelberg, Germany, 2019; pp. 32–58. [CrossRef] [PubMed]
21. Wallenberger, F.T.; Bingham, P.A. *Fiberglass and Glass Technology: Energy-Friendly Compositions and Applications*; Springer: Boston, MA, USA, 2010.
22. Krauklis, A.E.; Gagani, A.I.; Echtermeyer, A.T. Long-Term Hydrolytic Degradation of the Sizing-Rich Composite Interphase. *Coatings* **2019**, *9*, 263.
23. Thomason, J.L. Glass fibre sizing: A review. *Compos. Part A-Appl. S.* **2019**, *127*, 105619. [CrossRef]
24. Filho, O.P.; La Torre, G.P.; Hench, L.L. Effect of crystallization on apatite-layer formation of bioactive glass 45S5. *J. Biomed. Mater. Res.* **1996**, *30*, 509–514. [CrossRef]
25. Arstila, H.; Vedel, E.; Hupa, L.; Hupa, M. Factors affecting crystallization of bioactive glasses. *J. Eur. Ceram. Soc.* **2007**, *27*, 1543–1546. [CrossRef]
26. Liu, X.; Rahaman, M.N.; Hilmas, G.E.; Bal, B.S. Mechanical properties of bioactive glass (13-93) scaffolds fabricated by robotic deposition for structural bone repair. *Acta Biomater.* **2013**, *9*, 7025–7034. [CrossRef]
27. Jenkins, P.G. Understanding physical changes and strength loss of E-glass fibres following exposure to elevated temperatures. *Mater. Sci. Technol.* **2016**, *33*, 255–264. [CrossRef]
28. Mishra, A.; Désévédavy, F.; Petit, L.; Smektala, F.; Massera, J. Core-clad phosphate glass fibers for biosensing. *Mat. Sci. Eng. C* **2019**, *96*, 458–465. [CrossRef]
29. Pirhonen, E.; Törmälä, P. Coating of bioactive glass 13-93 fibres with biomedical polymers. *J. Mater. Sci.* **2006**, *41*, 2031–2036. [CrossRef]
30. Lehtonen, T.J.; Tuominen, J.U.; Hiekkanen, E. Dissolution behavior of high strength bioresorbable glass fibers manufactured by continuous fiber drawing. *Mater. Sci. Technol.* **2013**, *20*, 376–386. [CrossRef]
31. Vedel, E. Predicting physical and chemical properties of bioactive glasses from chemical composition. Part 1: Viscosity characteristics. *Glass Tech. Eur. J. Glass Sci. Technol. A* **2008**, *49*, 251–259. [CrossRef]
32. Vedel, E. Predicting physical and chemical properties of bioactive glasses from chemical composition. Part 4: Tailoring compositions with desired properties. *Glass Tech. Eur. J. Glass Sci. Technol. A* **2009**, *50*, 9-16.
33. Baranowska, A.; Dabrowski, J.R.; Dorosz, J. Thermal and mechanical properties of bioactive glass fibers for nanocomposites. In *Photonics Application in Astronomy, Communications, Industry, and High-Energy Physics Experiments*; SPIE—International Society for Optics and Photonics: Bellingham, WA, USA, 2018; Volume 32, pp. 2757–2774.
34. Scholze, H. Der Einfluß von Viskosität und Oberflächenspannung auf erhitzungsmikroskopische Messungen an Gläsern. *Ber. Dtsch. Keram. Ges.* **1962**, *39*, 63–68.
35. Quinn, J.B.; Quinn, G.D. A practical and systematic review of Weibull statistics for reporting strengths of dental materials. *Dent. Mater.* **2010**, *26*, 135–147.
36. Kokubo, T.; Takadama, H. How useful is SBF in predicting in vivo bone activity? *Biomaterials* **2006**, *27*, 2907–2915. [CrossRef]
37. Boccaccini, A.; Hamann, B. Review: In Situ high-temperature optical microscopy. *J. Mater. Sci.* **1999**, *34*, 5419–5436. [CrossRef]
38. Mishra, A. *Phosphate Glasses and Fibers as an Alternative to Silicate Bioactive Glasses*; Academic Dissertation: Tampere, Finland, 2019. [CrossRef]
39. Fagerlund, S.; Hupa, L. Melt-derived Bioactive Silicate Glasses. In *Bioactive glasses: Fundamentals, Technology and Applications*; Boccaccini, A.R., Brauer, D.S., Hupa, L., Eds.; Royal Society of Chemistry: Cambridge, UK, 2017; Chapter 1, pp. 1–26.
40. Pirhonen, E.; Niiranen, H.; Niemelä, T.; Brink, M.; Törmälä, P. Manufacturing, mechanical characterization, and *in vitro* performance of bioactive glass 13–93 fibers. *J. Biomed. Mater. Res.* **2006**, *77*, 227–233.
41. Colquhoun, R.; Tanner, K.E. Mechanical behaviour of degradable phosphate glass fibres and composites—A review. *Biomed. Mater.* **2016**, *11*, 014105. [CrossRef]
42. Vallittu, P.K.; Narva, K. Impact strength of a modified continuous glass fiber-poly(methyl methacrylate). *Int. J. Prosthodont.* **1997**, *10*, 142–148. [CrossRef]